*Inorg. Chem.* **2004**, *43*, 6151–6158

# The Nowotny Chimney Ladder Phases: Following the $c_{pseudo}$ Clue toward an Explanation of the 14 Electron Rule

**Daniel C. Fredrickson,[†] Stephen Lee,*[,†,‡] Roald Hoffmann,*[,†] and Jianhua Lin[‡]**

*Department of Chemistry and Chemical Biology, Baker Laboratory, Cornell University, Ithaca, New York 14853-1301, and State Key Laboratory for Rare Earth Chemistry and Applications, College of Chemistry and Molecular Engineering, Peking University, Beijing, 100871, China*

Received May 3, 2004

We account for two empirical rules of the Nowotny chimney ladder phases (NCLs, intermetallic compounds of the form $T_tE_m$; T, groups 4–9; E, groups 13–15). The first rule is that for late transition metal NCLs the total number of valence electrons per T atom is 14. The second is the appearance of a pseudoperiodicity with a spacing, $\mathbf{c}_{pseudo}$, which is directly related to the stoichiometry, $T_tE_m$, by $(2t - m)\,\mathbf{c}_{pseudo} = \mathbf{c}$. Both rules are accounted for by viewing the NCLs as twinned structures constructed from blocks of the parent compound, $RuGa_2$ of thickness $\mathbf{c}_{pseudo}/2$, with the successive layers rotated relative to each other by 90°. Sterically encumbered E atoms are then deleted at the interfaces between layers, followed by relaxation.

## 1. The Nowotny Chimney Ladders

The Nowotny chimney ladder phases (NCLs)[1] are a series of intermetallic structures formed between transition metal elements (T, groups 4, 5, 6, 7, 8, and 9) and main group elements (E, groups 13, 14, with recent examples of group 15[2,3]). Behind their relatively simple stoichiometries, $T_tE_m$, is an exquisite blend of structural complexity with simple experimental and theoretical stability rules. In this paper, setting out from the structures of these phases, we begin to construct theoretical explanations for the rules governing their structures and electron counts.

We commence with the traditional view of these structures, taking $Ru_2Sn_3$ as an example.[4] One unit cell of this compound is shown in Figure 1a. In this figure, the T atoms are shown as red spheres, and the E atoms are shown as blue spheres.

The T atoms form a tetragonal sublattice. In the projection shown in Figure 1a, this tetragonal sublattice resembles a square net. Viewed perpendicular to Figure 1a, i.e., along the **a** or **b** axis, each square unfolds to a 4-fold helix, as shown in Figure 1b. We denote the period of this helix as $\mathbf{c}_t$. One of these helices is emphasized in Figure 1a, with the heights of the T atoms indicated for one period. The helix segment shown begins at height 0 and twists counterclockwise through atoms at heights $^1/_4\mathbf{c}_t$, $^1/_2\mathbf{c}_t$, $^3/_4\mathbf{c}_t$, and finally back to $1\mathbf{c}_t$. Neighboring helices are interconnected, with each T atom shared among four helices. This arrangement of atoms is also seen in the $\beta$-Sn structure. It is conserved throughout the NCL series.

A second structural component is composed of the E atoms. These atoms are shown as blue spheres for the $Ru_2Sn_3$ structure[4] in Figure 1a. Viewed down the **c** axis, the E atoms appear as discrete triangular units, embedded in the channels formed by the interiors of the T atom helices. In Figure 1b, we show that along **c** these triangular units stretch out into 3-fold helices. The distance along **c** between neighboring atoms in the helix is denoted as $\mathbf{c}_m$. Thus, the repeat vector for the helix is $3\mathbf{c}_m$. The heights (along **c**) for one helix are given in Figure 1a; here the heights are given with respect to the underlying T atom sublattice. The repeating $E_3$ unit begins at height $0.50\mathbf{c}_t$, progresses counterclockwise through heights $1.16\mathbf{c}_t$ and $1.84\mathbf{c}_t$, and finishes at height $2.50\mathbf{c}_t$. The rise over one period is then $2.0\mathbf{c}_t$. This is equal to two periods of the T atom sublattice.

We now see a beautiful structural feature of the NCL structures. Both the structural components form regularly spaced structures along **c**. However, the spacings of these two components are different. The repeat distance of E atom

* Authors to whom correspondence should be addressed. E-mail: sl137@cornell.edu (S.L.) or rh34@cornell.edu (R.H.).
† Cornell University.
‡ Peking University.

(1) Nowotny, H. Crystal Chemistry of Transition Element Defect Silicides and Related Compounds. In *The Chemistry of Extended Defects in Nonmetallic Solids*; Eyring, L., O'Keeffe, M., Eds.; North-Holland Publishing Co.: Amsterdam and London, 1970.
(2) Kleinke, H. *Inorg. Chem.* **2001**, *40*, 95−100.
(3) Elder, I.; Lee, C.-S.; Kleinke, H. *Inorg. Chem.* **2002**, *41*, 538−545.
(4) Schwomma, O.; Nowotny, H.; Wittmann, A. *Monatsh. Chem.* **1964**, *95*, 1538−1543.

10.1021/ic049427n CCC: $27.50 
Published on Web 06/29/2004

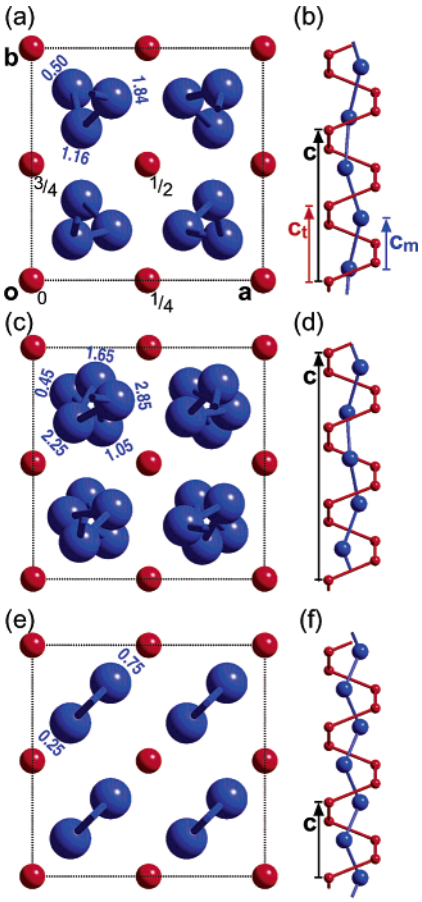


**Figure 1.** Nowotny chimney ladder structures: the (a,b) $Ru_2Sn_3$, (c,d) $Ir_3Ga_5$, and (e,f) $TiSi_2$ (exemplified by $RuGa_2$) structure types. In each structure, the T atoms are shown as small red balls, while the E atoms are shown as large blue balls.

sublattice ($3\mathbf{c}_m$, one turn of the E atom helix) is twice the repeat distance of the T atom sublattice ($\mathbf{c}_t$).

A similar situation occurs in the other NCL structures. As two further structural examples, we take the $Ir_3Ga_5$[5] and $RuGa_2$[6,7] structures. $Ir_3Ga_5$ is illustrated in Figure 1c. Here, the E atoms appear to trace out a five-pointed star over one period. As shown in Figure 1d, it is actually a helix, containing five E atoms, with a repeat equal to three times the repeat distance of the T sublattice.

The $RuGa_2$ structure is shown in Figure 1e and Figure 1f. The E atoms form 2-fold helices, which are, of course, zigzag chains. In this structure, the periods of the T and E sublattices coincide: the repeat distance of the E sublattice is equal to the repeat distance of the T sublattice. In this sense and in many others, as we shall see, $RuGa_2$ is a parent structure for the Nowotny chimney ladders.

The aesthetic appeal of helices (even before the α-helix and DNA) is so strong that one is seduced to seek structural and electronic rationales in these incredibly beautiful helices within helices. As we will soon see, a productive structural and electronic analysis points elsewhere.

**Table 1.** Binary Nowotny Chimney Ladder Phases (T from Group 7 or Higher)

| compound | structure type | $e^-/T$ | reference |
|---|---|---|---|
| $Ru_2Sn_3$ | $Ru_2Sn_3$ | 14 | Schwomma et al.[4] |
| | $Ru_2Ge_3$[a] | 14 | Poutcharovsky et al.[18] |
| $Ir_3Ga_5$ | $Ir_3Ga_5$ | 14 | Völlenkle et al.[5,19] |
| $RuGa_2$ | $TiSi_2$ | 14 | Jeitschko et al.,[6] Evers et al.[7] |
| $RuAl_2$ | $TiSi_2$ | 14 | Edshammar[20] |
| $Ru_2Ge_3$ | $Ru_2Ge_3$ | 14 | Poutcharovsky and Parthé,[21] Völlenkle[22] |
| | $Ru_2Sn_3$[b] | 14 | Poutcharovsky et al.[18] |
| $Ru_2Si_3$ | $Ru_2Ge_3$ | 14 | Poutcharovsky and Parthé,[21] Völlenkle[22] |
| | $Ru_2Sn_3$[b] | 14 | Poutcharovsky et al.[18] |
| $Os_2Ge_3$ | $Ru_2Ge_3$ | 14 | Poutcharovsky and Parthé,[21] Völlenkle[22] |
| $Os_2Si_3$ | $Ru_2Ge_3$ | 14 | Poutcharovsky and Parthé,[21] Völlenkle[22] |
| $Rh_{10}Ga_{17}$ | $Rh_{10}Ga_{17}$ | 14.1 | Völlenkle et al.[5,19] |
| $Rh_{17}Ge_{22}$ | $Rh_{17}Ge_{22}$ | 14.18 | Jeitschko and Parthé[8] |
| $Mn_4Si_7$ | $Mn_4Si_7$ | 14 | Karpinskii and Evseev[23] |
| $Tc_4Si_7$ | $Mn_4Si_7$ | 14 | Wittmann and Nowotny[24] |
| $Re_4Ge_7$ | $Mn_4Si_7$[d] | 14 | Larchev and Popova[25] |
| $Mn_{11}Si_{19}$ | $Mn_{11}Si_{19}$ | 13.96 | Schwomma et al.,[26] Knott et al.[27] |
| $Mn_{15}Si_{26}$ | $Mn_{15}Si_{26}$ | 13.93 | Flieher et al.[28] |
| $Mn_{27}Si_{47}$ | $Mn_{27}Si_{47}$ | 13.90 | Zwilling and Nowotny[29] |
| $Mn_{26}Si_{45}$ | $Mn_{26}Si_{45}$ | 13.92 | Flieher et al.[28] |
| $Mn_3Ge_5$ | $Mn_{11}Si_{19}$[c] | 13.67 | Takizawa et al.[30] |
| $Ir_4Ge_5$ | $Ir_4Ge_5$ | 14 | Panday et al.,[31] Flieher et al.[32] |
| $Co_2Si_3$ | $Ru_2Sn_3$[d] | 15 | Larchev and Popova[25] |
| $OsGa_2$ | $TiSi_2$[d] | 14 | Popova and Fomicheva[33] |

[a] Low-temperature phase. [b] High-temperature phase. [c] High-pressure phase. [d] High-temperature, high-pressure phase.

## 2. Two Empirical Rules for the NCL Phases

There are two rules that have been empirically observed for these phases. The first is an electron counting rule. The stability of a phase seems to be intimately related to the total number of valence electrons per transition metal atom. For transition metal groups 7, 8, and 9, there is a preponderance of structures with 14 valence electrons per transition metal.[8,9] We give examples of this in Table 1. The first example is $Ru_2Sn_3$ (Figure 1a), in which each Ru atom contributes eight electrons (the atoms being counted as neutral), and each Sn atom brings four electrons. The total number in each formula unit is then $2 \times 8 + 3 \times 4 = 28$ electrons. As there are two Ru atoms in the structure, this makes $^{28}/_2$, or 14 electrons per Ru atom. Two further examples of 14 electron compounds are $Ir_3Ga_5$ and $RuGa_2$ (respectively in Figure 1c and Figure 1e). Lu et al. has prepared a virtually continuous series of structures with 14 electrons of the form $RuGa_wSn_v$, with $8 + 3w + 4v = 14$.[10] Theoretical studies, ranging from empirical tight-binding to LDA-DFT calculations, associate this magic electron count with a minimum or gap in the density of states at this band filling.[11−17] However, no explanation has been proffered for *why* this minimum or gap occurs consistently at 14 electrons per T atom and does not shift with changes in the stoichiometry. In this series of papers, we will forge a chemical explanation for the 14 electron rule.

A second rule is discernible in the electron diffraction of the NCLs. In the course of studies on the electron diffraction patterns of Mn−Si NCLs, Amelinckx and co-workers found

(5) Völlenkle, H.; Wittmann, A.; Nowotny, H. *Monatsh. Chem.* **1967**, *98*, 176−183.
(6) Jeitschko, W.; Holleck, H.; Nowotny, H.; Benesovsky, F. *Monatsh. Chem.* **1963**, *94*, 838−840.
(7) Evers, J.; Oehlinger, G.; Meyer, H. *Mater. Res. Bull.* **1984**, *19*, 1177−1180.
(8) Jeitschko, W.; Parthé, E. *Acta Crystallogr.* **1967**, *22*, 417−430.
(9) Pearson, W. B. *Acta Crystallogr.* **1970**, *B26*, 1044−1046.
(10) Lu, G.; Lee, S.; Lin, J.; You, L.; Sun, J.; Schmidt, J. T. *J. Solid State Chem.* **2002**, *164*, 210−219.

that, in addition to main reflections from the T substructure, there were regularly spaced satellites arising from the mismatch of the T and E atom components.[34,35] We'll call the spacing between the satellite peaks $\mathbf{c}^*_{pseudo}$. These satellites were particularly clear in images down the [110] direction of the samples. They also found a relationship between $\mathbf{c}^*_{pseudo}$ and the stoichiometry of the NCL phase, $Mn_tSi_m$. In reciprocal space, this relationship states that $\mathbf{c}^*_{pseudo}$ is a multiple of $\boldsymbol{c}^*$, with the relation

$$\mathbf{c}^*_{pseudo} = (2t - m)\mathbf{c}^* \quad (1)$$

where again, t and m are respectively the number of T (Mn) and E (Si) atoms in the stoichiometric formula of the compound.[35] This relationship between the reflection positions and the stoichiometry is consistent with a reflection condition derived by Boller based on the helical nature of the NCLs.[36] The division of these reflections into main and satellite reflections has been elegantly used to simplify the structure solution of the NCL phases, through the modulated composite crystal approach.[37,38] As we show below, this division is deeply rooted in the electron counting rule for these phases.


(11) Pécheur, P.; Toussaint, G. *Phys. Lett. A* **1991**, *160*, 193−196.
(12) Pécheur, P.; Toussaint, G.; Kenzari, H.; Malaman, B.; Welter, R. *J. Alloys Compd.* **1997**, *262*−*263*, 363−365.
(13) Wolf, W.; Bihlmayer, G.; Blügel, S. *Phys. Rev. B* **1997**, *55*, 6918−6926.
(14) Filonov, A. B.; Migas, D. B.; Shaposhnikov, V. L.; Dorozhkin, N. N.; Borisenko, V. E.; Heinrich, A.; Lange, H. *Phys. Rev. B* **1999**, *60*, 16494−16498.
(15) Pécheur, P.; Tobola, J.; Kenzari, H.; Malaman, B.; Welter, R. *J. Alloys Compd* **2001**, *317*−*318*, 327−330.
(16) Krajčí, M.; Hafner, J. *J. Phys.: Condens. Matter* **2002**, *14*, 5755−5783.
(17) Krajčí, M.; Hafner, J. *J. Phys.: Condens. Matter* **2002**, *14*, 7201−7219.
(18) Poutcharovsky, D. J.; Yvon, K.; Parthé, E. *J. Less-Common Met.* **1975**, *40*, 139−144.
(19) Völlenkle, H.; Wittmann, A.; Nowotny, H. *Monatsh. Chem.* **1966**, *97*, 506−516.
(20) Edshammar, L.-D. *Acta Chem. Scand.* **1966**, *20*, 427−431.
(21) Poutcharovsky, D. J.; Parthé, E. *Acta Crystallogr.* **1974**, *B30*, 2692−2696.
(22) Völlenkle, H. *Monatsh. Chem.* **1974**, *105*, 1217−1227.
(23) Karpinskii, O. G.; Evseev, B. A. *Inorg. Mater.* **1969**, *5*, 438−442.
(24) Wittmann, A.; Nowotny, H. *J. Less-Common Met.* **1965**, *9*, 303−304.
(25) Larchev, V. I.; Popova, S. V. *J. Less-Common Met.* **1982**, *84*, 87−91.
(26) Schwomma, O.; Preisinger, A.; Nowotny, H.; Wittmann, A. *Monatsh. Chem.* **1964**, *95*, 1527−1537.
(27) Knott, H. W.; Mueller, M. H.; Heaton, L. *Acta Crystallogr.* **1967**, *23*, 549−555.
(28) Flieher, G.; Völlenkle, H.; Nowotny, H. *Monatsh. Chem.* **1967**, *98*, 2173−2179.
(29) Zwilling, G.; Nowotny, H. *Monatsh. Chem.* **1973**, *104*, 668−675.
(30) Takizawa, H.; Sato, T.; Endo, T.; Shimada, M. *J. Solid State Chem.* **1987**, *68*, 234−238.
(31) Panday, P. K.; Singh, G. S. P.; Schubert, K. *Z. Kristallogr., Kristallgeom., Kristallphys., Kristallchem.* **1967**, *125*, 274−285.
(32) Flieher, G.; Völlenkle, H.; Nowotny, H. *Monatsh. Chem.* **1968**, *99*, 877−883.
(33) Popova, S. V.; Fomicheva, L. N. *Inorg. Mater.* **1982**, *18*, 205−208.
(34) Ridder, R. D.; Amelinckx, S. *Mater. Res. Bull.* **1971**, *6*, 1223−1234.
(35) Ye, H. Q.; Amelinckx, S. *J. Solid State Chem.* **1986**, *61*, 8−39.
(36) Boller, H. *Monatsh. Chem.* **1974**, *105*, 934−943.
(37) Rohrer, F. E.; Lind, H.; Eriksson, L.; Larsson, A.-K.; Lidin, S. *Z. Kristallogr.* **2001**, *216*, 190−198.
(38) Rohrer, F. E.; Lind, H.; Eriksson, L.; Larsson, A.-K.; Lidin, S. *Z. Kristallogr.* **2000**, *215*, 650−660.


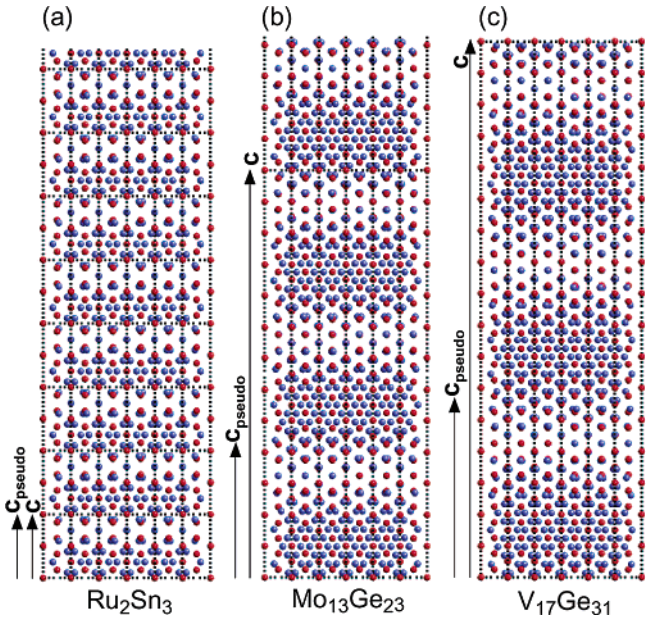


**Figure 2.** Views along [110] of three NCL phases (taking 3 unit cells along **a** and **b**): (a) $Ru_2Sn_3$, (b) $Mo_{13}Ge_{23}$, and (c) $V_{17}Ge_{31}$. For each structure **c** and $\mathbf{c}_{pseudo} = \mathbf{c}/(2t - m)$ are indicated. Transition metals are in red, main group atoms in blue.

In real space, $\mathbf{c}_{pseudo}$ corresponds to a modulation in the structure, due to the mismatch between the T atom and E atom components of the structure. There are an integer number of repeats of $\mathbf{c}_{pseudo}$ in the unit cell for the phase, with this number being 2t − m, i.e.,

$$(2t - m)\mathbf{c}_{pseudo} = \mathbf{c} \quad (2)$$

Lu et al. found $\mathbf{c}_{pseudo}$ satellites in the electron diffraction patterns of NCLs of the form $RuGa_wSn_v$, and established that the 2t − m rule held for these structures as well. Through inspection of a number of other NCL structures, they concluded that the existence of $\mathbf{c}_{pseudo}$ is a general phenomenon in the NCLs.[10]

As examples of this second experimental rule, we can again take the NCLs shown in Figure 1. For $Ru_2Sn_3$ (Figure 1a), $2t - m = 2 \times 2 - 3 = 1$, and there $\mathbf{c}_{pseudo}$ coincides with **c**. For $Ir_3Ga_5$ (Figure 1c), $2t - m = 2 \times 3 - 5 = 1$, and again $\mathbf{c}_{pseudo}$ is equal to **c**. For $RuGa_2$ (Figure 1e), $2t - m = 2 \times 1 - 2 = 0$, and there is no $\mathbf{c}_{pseudo}$. The absence of $\mathbf{c}_{pseudo}$ is another sense in which $RuGa_2$ is a parent structure to the NCLs.

### 3. The Structural Origin of $\mathbf{c}_{pseudo}$

$\mathbf{c}_{pseudo}$ is the key to unlocking the mystery of the 14 electron rule and the intriguing structures of the NCL phases. In seeking out its structural origins, we essay an alternative way to view the NCL structures, which deepens our understanding of these phases as defect $RuGa_2$ structures. In this paper we will explain the $\mathbf{c}_{pseudo}$ rule, and show its connections to the 14 electron rule.

The structural origin of $\mathbf{c}_{pseudo}$ was investigated by Lu et al. by viewing the structures down their [110] direction.[10] In Figure 2, we show such views for three NCL phases

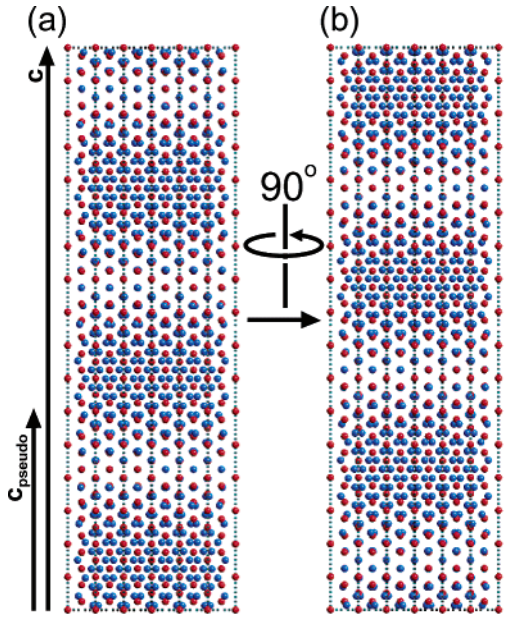


**Figure 3.** $\mathbf{c}_{pseudo}$ in $V_{17}Ge_{31}$. (a) View of $V_{17}Ge_{31}$ along [110]. An alternation of layers which appear dense in projection and layers which appear sparse in projection gives rise to an apparent periodicity. The average length along **c** of these repeats is $\mathbf{c}_{pseudo}$. (b) Upon rotating the structure by 90° about **c**, the layers which appeared sparse become dense in projection and vice versa. V: red. Ge: blue.

($Ru_2Sn_3$, $Mo_{13}Ge_{23}$,[39] and $V_{17}Ge_{31}$[39]). For each structure, a succession of layers is visible: there is an alternation of layers that appear dense in the projection shown with layers that appear sparse in the projection. The alternation of these layers gives rise to a pseudoperiodicity, with the apparent repeat unit consisting of one dense-looking layer and one sparse-looking layer. (Near the border between layers, the distinction becomes a little fuzzy. We'll turn our attention to this later in this paper.) The length of this pseudo repeat unit corresponds to $\mathbf{c}_{pseudo}$, while the true repeat distance of the structure is given by the crystallographic **c**. Following the rule noted above, there are 2t − m of these $\mathbf{c}_{pseudo}$ repeats per **c**. *The transition metal component of these structures, formed of 4-fold helices, passes unchanged through these layers*; the appearance of these alternating layers reflects the positions of the main group atoms.

Now, let's look more closely at what these layers are. In Figure 3a, we show a [110] view of $V_{17}Ge_{31}$. Again, the alternation of slabs which appear dense and sparse in projection is clearly seen. In this case there are 2t − m = 2(17) − 31 = 3 repeats of $\mathbf{c}_{pseudo}$ in the unit cell. When we rotate the structure about the **c** axis by 90°, we find the structure shown in Figure 3b. The same alternation of layers is seen in this rotated structure. However, the layers which appeared dense in Figure 3a appear sparse in Figure 3b, and vice versa. $V_{17}Ge_{31}$ can then be thought of as being derived from the stacking of these layers (some of different lengths than others), with each layer being rotated 90° relative to the layer above and below it. The layer appears sparse when, from our viewpoint, the atoms lie on top of each other in columns; the layer appears dense when we rotate it by 90°, and the atoms no longer hide each other.

(39) Völlenkle, V. H.; Preisinger, A.; Nowotny, H.; Wittmann, A. *Z. Kristallogr., Kristallgeom., Kristallphys., Kristallchem.* **1967**, *124*, 9−25.

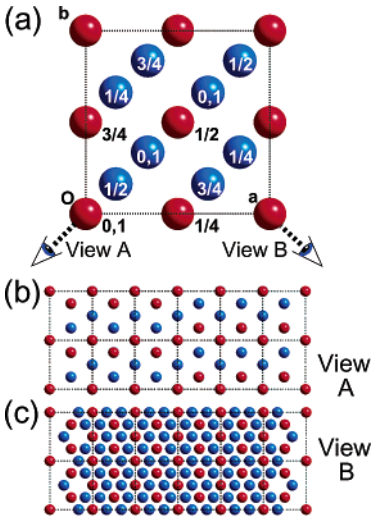


**Figure 4.** The $RuGa_2$ structure type. (a) Definitions of two views, view A and view B, of the structure. (b) View A of 3 × 3 × 1 unit cells of $RuGa_2$, resembling the sparse view of the layers in Figure 3a and Figure 3b. (c) View B of $RuGa_2$, resembling the dense view. Ru: red. Ga: blue.

To identify this layer, we turn to the simple $RuGa_2$ structure, where 2t − m = 0, and no $\mathbf{c}_{pseudo}$ should be present. We show this structure in Figure 4a−c, with views A (Figure 4b) and B (Figure 4c) corresponding to the views of $V_{17}Ge_{31}$ in respectively Figure 3a and Figure 3b. In accordance with the expectation that $RuGa_2$ should have no $\mathbf{c}_{pseudo}$, these views show no alternation of layers. The entirety of the structure in view A resembles the layers that are sparse in projection. View B closely resembles the layers of $V_{17}Ge_{31}$ that are dense in projection. The resemblance is very strong near the centers of the layers, and fades a little near the edges of the layers.

The connection between the complex NCL phases and the parent $TE_2$ ($RuGa_2$) structure now comes into focus. *The complex NCL phases consist of $TE_2$ slabs, with neighboring slabs rotated with respect to each other by 90°*. To complete this structural connection, we focus on the region between the $TE_2$ layers of a NCL phase. To see what happens here, let's take a simple case: $T_2E_3$ ($Ru_2Sn_3$). In Figure 5, we illustrate a hypothetical construction of this structure from $TE_2$ layers. We start in Figure 5a with one unit cell of $TE_2$, running from height 0 to $1\boldsymbol{c}_{TE_2}$, with the E atoms shown in blue. In Figure 5b, we show another unit cell of $TE_2$, running from height $1\boldsymbol{c}_{TE_2}$ to $2\boldsymbol{c}_{TE_2}$, with the E atoms shown in green. The structure in Figure 5b is rotated by 90° with respect to that in Figure 5a in such a direction that the T atom substructure (4-fold helix) can run uninterrupted from the structure in Figure 5a to the structure in Figure 5b. Now we fuse these two structures together to make a doubled $TE_2$ cell. The fused structure is shown in Figure 5c. In this structure the upper and lower layers are related by a $\bar{4}$ axis, with the inversion occurring about the T atom at height $1\boldsymbol{c}_{TE_2}$.

The fused structure has a number of unphysically small close E−E contacts of 1.7 Å between the atoms of the upper and lower $TE_2$ layers. These are shown by yellow connecting bars in Figure 5c. They exist between atoms of one slab at the interface (those at height $1\boldsymbol{c}_{TE_2}$) and the atoms of the

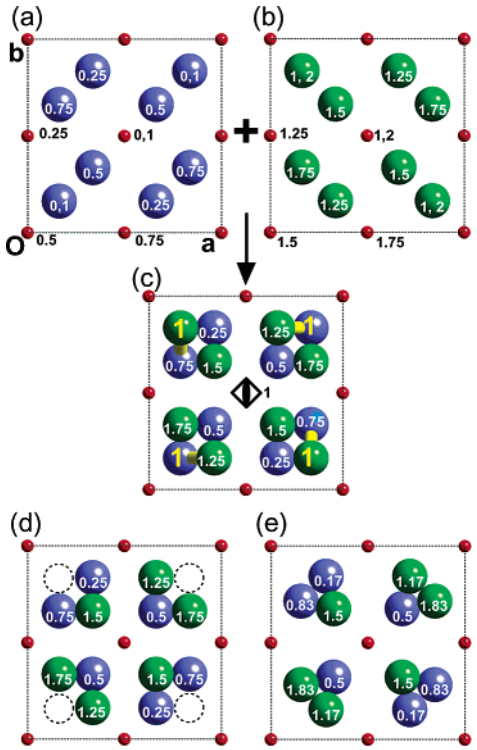


**Figure 5.** Construction of $T_2E_3$ ($Ru_2Sn_3$) from $TE_2$ ($RuGa_2$) layers. (a) One unit cell of $TE_2$ spanning heights $0\mathbf{c}_{TE_2}-1\mathbf{c}_{TE_2}$, with E atoms in blue (T atoms in red). (b) Another cell of $RuGa_2$ spanning heights $1\mathbf{c}_{TE_2}-2\mathbf{c}_{TE_2}$, with the Ga sublattice orientation changed by a 90° rotation about **c**, with E atoms in green. (c) The structure formed from the overlay of these two $TE_2$ to form a structure which spans heights $0\mathbf{c}_{TE_2}-2\mathbf{c}_{TE_2}$ (here $2\mathbf{c}_{TE_2}=\mathbf{c}$). The T atom component runs uninterrupted at the junction of parts a and b. The E atom component is reoriented by 90° at this junction, the actual relation between the blue and green parts being a $\bar{4}$ axis. The E atoms at the junction have unphysically close contacts to other E atoms (1.63 Å). (d) The structure derived from removing all of the E atoms at the junction, thus relieving the close contacts, creates a structure of stoichiometry $T_2E_3$. (e) The experimentally observed $Ru_2Sn_3$ structure type.

other slab $0.25\boldsymbol{c}_{\mathbf{TE_2}}$ above or below the interface. To alleviate this "steric" problem, *all* of the E sites at the interface (at $1\boldsymbol{c}_{\mathbf{TE_2}}$ in Figure 5) are vacated. Upon introducing these vacancies at the interfaces, the structure in Figure 5d, with stoichiometry $T_2E_3$, results. At each interface, there is a net loss of two E atoms.

Now we have everything we need to explain the 2t − m rule for $\mathbf{c}_{pseudo}$. For a phase $T_tE_m$, we can derive the expected value of $\mathbf{c}_{pseudo}$. First we take t cells of $TE_2$ structure along **c** to obtain a supercell with the contents $T_{4t}E_{8t}$. Next we count the number of interfaces that are necessary to produce the stoichiometry $4(T_tE_m) = T_{4t}E_{4m}$, remembering that at each interface two E atoms are lost. Taking *n* as the number of interfaces this gives us

$$T_{4t}E_{8t-2n} = T_{4t}E_{4m} \tag{3}$$

Solving for the number of interfaces, we find

$$n = 4t - 2m \tag{4}$$

Two interfaces are necessary for each $\mathbf{c}_{pseudo}$ repeat. The average thickness of each repeat will then be the length of the **c** axis, divided by half the number of interfaces, thus

$$\mathbf{c}_{pseudo} = \mathbf{c}/(n/2) = \mathbf{c}/(2t - m) \tag{5}$$

and

$$\mathbf{c} = (2t - m)\mathbf{c}_{pseudo} \tag{6}$$

The 2t − m rule for $\mathbf{c}_{pseudo}$ is then easily recovered with the observation that, at the interfaces between $TE_2$ layers, two E atoms per unit cell are lost.

In looking at the structures resulting from this idealized stacking of $TE_2$ slabs as shown for $T_2E_3$ in Figure 5, one sees clear differences from the experimental structures. What ensues may be viewed as analogous to the relaxation seen at the surfaces of solids,[40] with the main effects being in the E substructure. This is illustrated in a comparison of our idealized $T_2E_3$ structure in Figure 5d, with the experimental $T_2E_3$ ($Ru_2Sn_3$) structure in Figure 5e. Comparison of Figure 5d and Figure 5e shows that it is in the process of this relaxation that the beautiful main group atom helix appears in this scheme. In our calculations below, and in those of a future paper, we will assess the importance of this relaxation in determining the optimal electron counts for the NCL structures.

This explanation for the 2t − m rule for $\mathbf{c}_{pseudo}$ suggests that an NCL phase can be regarded as a stack of $TE_2$ slabs with E atom vacancies at the interfaces between the slabs.

This twinned $TE_2$ model has been hinted at in the observations of a number of earlier workers. The interpretation of complex solid state structures through chemical twinning is deeply ingrained in solid state chemistry.[41] Knott et al. provided an interpretation of the $Mn_{15}Si_{26}$ structure in terms of "pseudo-hexagonal sheets" of alternating orientation along **c**.[27] These sheets arise from the $TE_2$ stacking we describe here. Grin showed that the structures and space group symmetries of the NCLs can be accounted for by taking linear combinations of $T_2E_4$, $T_2E_2$, and $T_3E_4$ layers along **c**.[42] Our *Aufbau* is different, but parallels can be drawn: the first of Grin's layers corresponds to center portions of planes of the $TE_2$ structure in our picture. The others represent variations of the regions surrounding interfaces we describe here. Our discussion above traces these layers to the $TE_2$ structure and links this view to the $\mathbf{c}_{pseudo}$ rule.

An NCL can reduce the ratio of E to T atoms in the stoichiometry by creating more interfaces. This is motivated by the 14 electron rule. Consider for example a $Ru_xSn_y$ compound. It can't be $RuSn_2$ in the $RuGa_2$ structure, because that would have 16 electrons per Ru atom. But if one follows our *Aufbau*, rotating $RuSn_2$ blocks with respect to each other and eliminating some interface atoms, one gets to $(RuSn_2)(RuSn_2) - Sn = Ru_2Sn_3$, a 14 electron compound. This will be heralded by the appearance of $\mathbf{c}_{pseudo}$ at twice the distance between interfaces. We will trace this phenomenon in detail in the next sections.

(40) Somorjai, G. A. *Chemistry in Two Dimensions: Surfaces*; Cornell University Press: Ithaca, NY, 1981.
(41) Hyde, B. G.; Andersson, S. *Inorganic Crystal Structures*; John Wiley & Sons: New York, 1989.
(42) Grin, J. N. *Monatsh. Chem.* **1986**, *117*, 921−932.

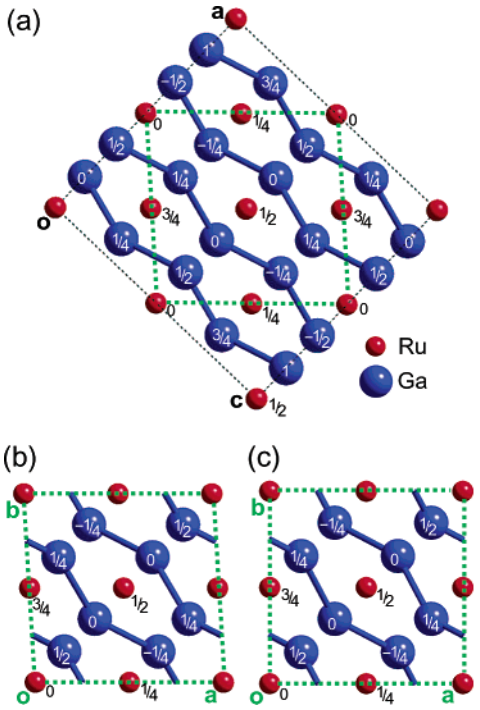


**Figure 6.** $RuGa_2$ in the $TiSi_2$ structure type. (a) The conventional unit cell for this structure. (b) The unit cell analogous to the NCL structures. (c) The idealization of the $RuGa_2$ structure to be studied here.

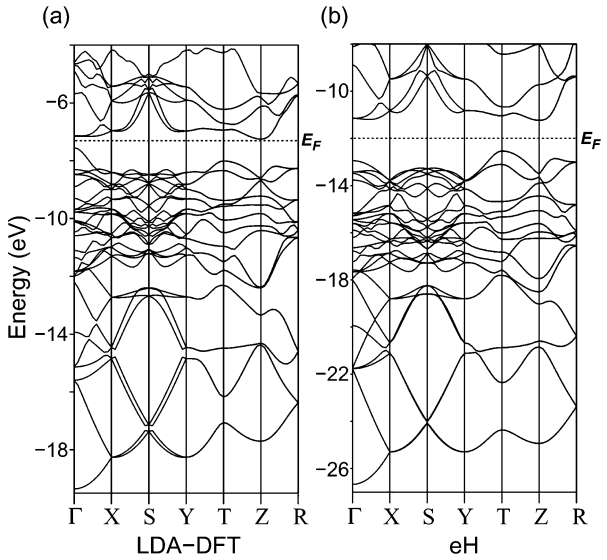


**Figure 7.** Band structures of the $RuGa_2$ structure type. (a) The band structure calculated for the experimental unit cell, as shown in Figure 2b, with LDA-DFT. (b) The band structure calculated for the idealized structure, as shown in Figure 2c, with the extended Hückel method. The dotted lines give the Fermi Energy ($E_F$) at 14 $e^-$/Ru.

## 4. The 14 Electron Rule: $RuGa_2$

From exploring the structural origins of $\mathbf{c}_{pseudo}$, we have found that the Nowotny chimney ladder phases may be seen as layers of $TE_2$ separated by interface regions. This provides a vital clue into how we can approach the electron counting rules for these phases: we begin by looking at the electronic structure of $TE_2$, and then turn to the effect of introducing the interfaces (and the relaxation which creates the E atom helices). First, let's look at why the 14 electron count is preferred for these phases.

The natural structure to start with is $RuGa_2$, the simplest structure in the Nowotny chimney ladder series, and a prototypical example of the 14 electron rule at work for these phases. Experimentally, it has been found to be a narrow-gap semiconductor with a band gap of about 0.42 eV.[7] A number of calculations on this structure type have shown band gaps at this electron count.[15−17]

As a first step toward a qualitative understanding of the 14 electron rule, we performed LDA-DFT band structure calculations on the experimental structure using the VASP package.[43−46] We must mention that in our calculations we are using an unconventional unit cell. $RuGa_2$ crystallizes in the $TiSi_2$ structure type.[47] Its space group is *Fddd*; the conventional unit cell, shown in Figure 6a, is face-centered. This unit cell is outlined with black, dotted lines. While conventional, it does not make the connection between this structure and the other Nowotny chimney ladders. To make this link, it is convenient to change unit cells. In Figure 6a, our new, NCL-type unit cell is outlined in green, and is shown individually in Figure 6b.

The LDA-DFT band structure is shown in Figure 7a. The Fermi energy ($E_F$) is at −7.31 eV in a narrow band opening, with an indirect band gap of about 0.33 eV. The smallest direct gap is about 0.39 eV and is at Γ. At other *k*-points, we see larger energy gaps between filled and unfilled states, typically of about 1 eV. The 14 electron rule is then associated with this band gap, in accord with classical molecular experience which correlates a gap with thermodynamic (and kinetic) stability.

For additional insight, we moved to extended Hückel (eH) calculations. These calculations have a history of providing qualitative explanations through a variety of perturbation theory based analytical tools associated with them.[48] As we will see in the accompanying publication,[49] this methodology will allow us construct a chemical explanation for the occurrence of a band gap at 14 $e^-$/Ru. We began by calculating the eH band structure of this phase using the Ru and Sn (for Ga, in preparation for studying other NCL structures, in particular $Ru_2Sn_3$) parameters traditionally employed in the study of molecules.[50] The resulting band structure (not shown here) gave noticeable differences from the LDA-DFT one, in particular no gap or opening in the band structure for the 14 electron count. Some modification of the Ru and Sn eH parameters is evidently necessary for studying transition metal−main group bonding in this intermetallic compound.

For each orbital type, there are several parameters which allow the tuning of an eH calculation. First, there is the

(43) Kresse, G.; Hafner, J. *Phys. Rev. B* **1993**, *47*, 55.
(44) Kresse, G.; Hafner, J. *Phys. Rev. B* **1994**, *49*, 14251.
(45) Kresse, G.; Furthmüller, J. *Comput. Mater. Sci.* **1995**, *6*, 15.
(46) Kresse, G.; Furthmüller, J. *Phys. Rev. B* **1996**, *54*, 11169.
(47) Jeitschko, W. *Acta Crystallogr.* **1977**, *B33*, 2347−2348.
(48) Hoffmann, R. *Solids and Surfaces: A Chemist's View of Bonding in Extended Structures*; VCH: New York, 1988.
(49) Fredrickson, D. C.; Lee, S.; Hoffmann, R. *Inorg. Chem.* **2004**, *43*, 6159−6167.
(50) Landrum, G. A. *YAeHMOP: Yet Another extended Hückel Molecular Orbital Package*, version 2.0b. YAeHMOP is freely available on the WWW at the URL http://sourceforge.net/projects/yaehmop/.

**Table 2.** Extended Hückel Parameters Used for Transition Metal (T) and Main Group (E) Atom Types

| orbital | $H_{ii}$ (eV) | $c_1$ | $\zeta_1$ | $c_2$ | $\zeta_2$ |
|---|---|---|---|---|---|
| T 5s | −10.40 | | 2.08 | | |
| T 5p | −6.87 | | 2.04 | | |
| T 4d | −14.90 | .5340 | 5.38 | .6365 | 1.80[a] |
| E 5s | −18.16[b] | | 2.12 | | |
| E 5p | −12.00[c] | | 1.82 | | |

[a] 2.30 in the standard Ru parameters. [b] −16.16 eV in the standard Sn parameters. [c] −8.32 eV in the standard Sn parameters.

ionization energy ($H_{ii}$) of each atomic orbital. Second, there are the exponents measuring the tightness or diffuseness of each atomic orbital ($\zeta$'s).

The eH Ru d band with standard parameters (for Ru and Sn) was substantially narrower than the DFT-calculated one. This suggested making the Ru d orbital more diffuse; we changed the long-range coefficient, $\zeta_2$, from 2.3 $Å^{-1}$ to 1.8 $Å^{-1}$ to obtain a closer match between the dispersion of the d bands at the two levels of theory.

The eH calculations also underestimated initially the energy spacing between the Ru d- and Sn s-type levels. This was remedied by shifting the Sn s and p $H_{ii}$'s down from −16.16 to −18.16 eV and from −8.32 to −11.32 eV, respectively. With these adjustments, the band structure in Figure 7b results. While some discrepancies between the LDA-DFT and this eH band structure remain, the overall qualitative agreement is excellent. These parameters are used in the remaining eH calculations in this paper. The entire set of eH parameters used in the sequel is listed in Table 2.

The eH band structure for $RuGa_2$ structure is shown in Figure 7b. We used a slightly idealized structure (Figure 6c) in anticipation of comparing our theoretical results on $RuGa_2$ to the other NCL phases. The following analysis refers consistently to this idealized structure. The $E_F$ for this band structure is at −11.99 eV. This lies in an indirect band gap of 1.22 eV, compared to the LDA-DFT gap of 0.33 eV, and experimental gap of 0.42 eV. The tendencies of eH theory to overestimate and for LDA-DFT to underestimate band gaps are well-known.

Below $E_F$, the gross features of the LDA-DFT and eH band structures are quite similar. Immediately below $E_F$, we find a series of rather narrow bands. There are in fact 20 of these bands. These arise from the d orbitals of the Ru atoms: four Ru atoms with five d orbitals each. Below this series of bands, there is a collection of bands with energy dispersions of several electronvolts. There are eight of these bands, coming from the s orbitals on the Ga atoms: eight Ga atoms in the unit cell, with one s orbital each. Altogether this makes 28 occupied bands, harboring 56 electrons per unit cell. With four Ru atoms in the unit cell, we recover 14 electrons per Ru atom.

### 5. The 14 Electron Rule: $Ru_2Sn_3$ and $Ir_3Ga_5$

From our LDA-DFT and eH calculations on $RuGa_2$ above, it is clear that the stability of this compound at 14 electrons arises from a large opening or a gap in the band structure at that electron count. Why this is so, in orbital and reciprocal space detail, will be explained in the accompanying paper, where we will also point to the connection between that magic electron count and the 18-electron rule for discrete organometallics.[49]

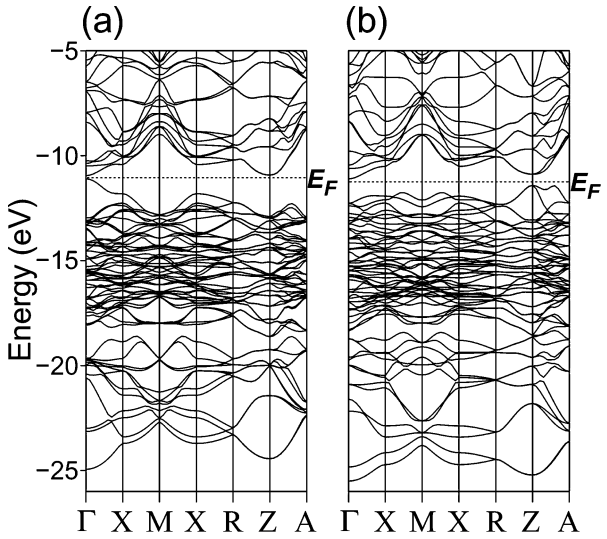


**Figure 8.** eH Band structures of (a) the observed $T_2E_3$ structure, and (b) an idealized structure of $T_2E_3$ formed from rotated slabs of $TE_2$ with deletions at the interfaces. The $E_F$ shown corresponds to a band filling of 14 electrons per T atom. In both the observed and idealized structures, the $E_F$ falls in an opening in the band structure.

Here we want to see how the gap at 14 electrons/T is preserved for the other NCLs. Calculations on $T_2E_3$ NCLs indicate that a similar opening in the band structure accounts for the stability of 14 electrons per T atom in these compounds as well. Let's tie this in with the clue $\mathbf{c}_{pseudo}$ gives us, that the complex NCL phases are composed of rotated slabs of the $TE_2$ structure, with deletions enforced, by unreasonably close contacts, at the layer interfaces. To this end, we can compare the band structures of NCL phases with those constructed of $TE_2$ layers as in Figure 5a−d, without any reconstruction. As specific examples we will take $T_2E_3$ ($Ru_2Sn_3$ type, Figure 1a) and $T_3E_5$ ($Ir_3Ga_5$ type, Figure 1b).

The eH band structure of the known $Ru_2Sn_3$ structure type is shown in Figure 8a. The $E_F$ lies in the center of a small band gap at −11.24 eV. This gap is consistent with the stability of these phases at 14 electrons per T atom. We should note however, that our eH calculation exaggerates this gap. $Ru_2Sn_3$ is known to be metallic, rather than semiconducting as our eH calculations suggest. An investigation of this phase with LDA-DFT calculations (not shown here) gives an opening in the density of states around the $E_F$, but it is not a true gap: the highest occupied state at Γ in eH penetrates through the opening in LDA-DFT. Despite this discrepancy, eH still illustrates clearly the propensity of this phase for 14 electrons per T atom.

Now let's consider the idealized $T_2E_3$ structure shown in Figure 5d (with vacancies at the interfaces, before relaxation). The resulting band structure is illustrated in Figure 8b, alongside the bands calculated for the observed geometry of the phase. In comparing the two band structures, we see some differences, but the overall forms of the bands are quite similar. The important comparison to make here is the region

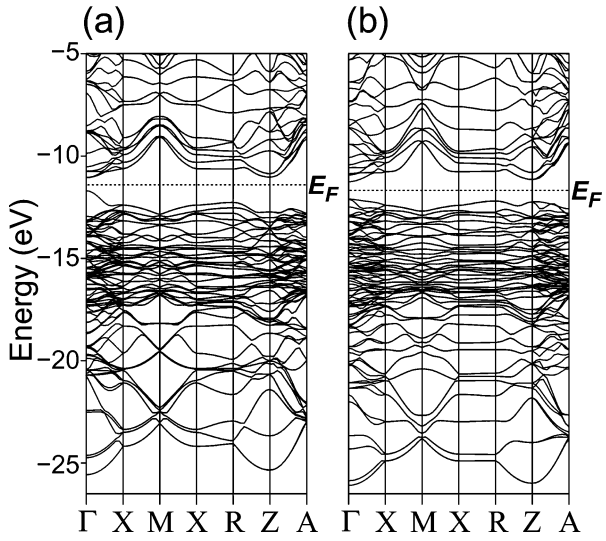


**Figure 9.** eH Band structures of (a) the observed $T_3E_5$ structure, and (b) an idealized structure of $T_3E_5$ formed from rotated slabs of $TE_2$ with deletions at the interfaces. The $E_F$ shown corresponds to a band filling of 14 electrons per T atom. In both the observed and idealized structures, the $E_F$ falls in an opening in the band structure.

around the $E_F$. The $E_F$ lies in a band gap in both structures. The band gap of the idealized structure (rotated blocks with deletions at the interfaces) is a little larger compared to the gap calculated for the observed structure (0.37 eV compared to 0.26 eV). The occurrence of the gap in the idealized structure (before the $E_3$ helices are formed) suggests strongly that the impetus for the 14 electron rule has its sources in the idealized model we forward, and not in the helicity of the E sublattice. The details of the interface relaxation will be given in a separate paper.

The same thing is found for the $Ir_3Ga_5$ structure type. We calculated band structures for the experimental structure and an idealized stacking of $TE_2$ layers (constructed in the same manner as for $T_2E_3$ in Figure 5a−d). The results for the experimental and idealized structures are given in respectively Figure 9a and Figure 9b. $E_F$ lies in a band gap in both band structures. Again, the gap for the idealized case is a little larger than for the observed structure (0.89 eV compared to 0.73 eV).

### 6. Onward and Upward with the 14 Electron Rule

From these examples we see that the band gap at 14 electrons per T atom in the $TE_2$ structure is obtained following the construction algorithm: (a) take $TE_2$ blocks of varying thickness; (b) rotate every other layer by 90° at the interfaces; (c) fuse the blocks, removing unphysically close atoms. Further relaxation, forming E sublattice helices, follows. From this observation, we can sketch how the 14 electron rule works for the NCLs, taking as an example the hypothetical construction of $Ru_2Sn_3$ from $RuGa_2$.

First, we consider the $RuGa_2$ structure with 14 electrons per Ru atom (we use Ru and Ga rather than T and E to keep track of how many valence electrons each atom brings to the structure). The stability of this structure is accounted for by the presence of a band gap at this electron count, the source of which we will explain in detail in a separate paper.[49] Each unit cell contains four formula units, so the actual cell contents are $4(RuGa_2) = Ru_4Ga_8$. We will insert interfaces following the pattern given in Figure 5: one interface at the bottom of each unit cell. In preparation for doing this, which will rotate every other unit cell by 90°, we double the unit cell along **c**, leaving us with the cell contents $(Ru_4Ga_8)(Ru_4Ga_8)$.

We now make the interfaces. Our doubled unit cell contains two interfaces, and two Ga atoms are lost at each interface. In order to keep the 14 electron count, the number of electrons must not change as we form the interfaces; when taking out a Ga atom, we must leave all of its electrons behind. This means that actually we are removing two $Ga^{3+}$ ions at each interface, four in all. The remaining structure is then $(Ru_4Ga_{8-2})^{2(3-)}(Ru_4Ga_{8-2})^{2(3-)} = (Ru_4Ga_6)^{6-}(Ru_4Ga_6)^{6-}$, or $Ru_2Ga_3^{3-}$. We can make a charge-neutral structure from this by noting that $Ga^-$ is isoelectronic with Sn. This gets us to $Ru_2Sn_3$, another 14 electron compound. The electrons left behind by the vacancies have been accommodated by the structure with the interfaces.

The same approach can be used for conceptually making $Ir_3Ga_5$ from $RuGa_2$. Briefly, the structure resulting from the insertion of interfaces has the composition $Ru_3Ga_5^{3-}$. We can regain charge neutrality by replacing three $Ga^-$ anions with Sn, or by replacing three $Ru^-$ anions with isoelectronic Ir atoms. Making the latter substitution gives us $Ir_3Ga_5$.

The construction algorithm we present here not only accounts for the $\mathbf{c}_{pseudo}$ regularity but also gives us an electronic justification for the 14 electron rule for the more complex structures (once we understand the reason for the 14 electron magic count for the parent $RuGa_2$ system).

**Acknowledgment.** We are grateful to Drs. Mikhail Shatruck and Lan-Feng Yuan for interesting discussions on the Nowotny chimney ladder compounds. We are also grateful for the financial support of the National Science Foundation (through Grant DMR-007358) and the Petroleum Research Fund.

IC049427N